Hydrofracturing tests on granite samples using a true triaxial device equipped with acoustic emission sensors

Hydrofracturing tests on granite samples using a true triaxial device equipped with acoustic emission sensors

M Herbón-Penabad*[1], A Muñoz-Ibáñez[1], J Delgado-Martín[1], N González-Molano[2], J Alvarellos-Iglesias[2] and J Canal-Vila[2]

[1] School of Civil Engineering, University of A Coruña, Campus de Elviña s/n, 15071 A Coruña, Spain
[2] Repsol Technology Lab, Ctra. Extremadura, N-V Km 18, 28935 Móstoles, Madrid (Spain)

miguel.herbon@udc.es

Abstract. We present a series of tests performed on granite samples using a true triaxial device designed and built at the Rock Mechanics Laboratory (University of A Coruña). The experiments were performed using cubic rock samples of 150 mm-edge, which were loaded to different stress conditions ($\sigma_h \leq \sigma_H \leq \sigma_V \leq 45$ MPa) on each loading axis. The device is based on a stiff steel frame that can be coupled to a servo-hydraulic testing machine that provides de vertical stress (σ_v), while two high-pressure pumps are used to deliver the lateral stress (σ_H and σ_h). An additional high-pressure pump is used to inject the fluid (mineral oil) into the rock sample at a low constant-flow rate. The aluminium loading platens, which are bevelled at the edges to avoid interaction among adjacent faces, have holes and grooves to introduce acoustic emission sensors that allow the location of fracture propagation. The specimens were drilled using a 6 mm drill bit until reaching the geometrical centre. Then, a 1/8'' (~3.18 mm) stainless steel tube is glued to the samples with epoxy. Strain measurements during the experiments were conducted using four strain gages attached to the orthogonal faces of the specimens. The system was further equipped with three LVDTs to account for the bulk displacement on each axis. Our results suggest a linear relationship between the breakdown pressure and the confining stress under hydrostatic conditions but no clear correlation in non-hydrostatic stress regime.

1. Introduction

The existence of exploitable underground oil and gas reserves is of great importance for the oil industry [1]. In the exploitation of unconventional reservoirs, in which formations with low permeability complicates resource recovery, hydrofracturing can be used to develop new paths for fluid displacement [2]. In order to get accurate results in laboratory-scale hydraulic fracturing tests, the samples should be subjected to stress conditions similar to those encountered in the field. In this work we perform hydrofracturing tests under true triaxial conditions (i.e., stress is applied in the three loading axes independently) using cubic (150 mm-edge) granite samples. Tests are carried out in a specially-designed frame coupled to a servo-hydraulic press. A comprehensive description of this system can be found in Muñoz-Ibáñez et al [3]. We study the potential relationship between the applied stress conditions and the value of breakdown pressure at which fractures are developed, and we take advantage of the acoustic emission (AE) technique to monitor the hydrofracturing processes.

2. Methods and materials

2.1. Materials and samples

Experiments were performed using samples of Blanco Mera granite, which is a coarse-grained (1–6 mm) rock of moderate strength. Properties of this material have been previously reported elsewhere [4-6], and a short summary is given in table 1.

Table 1. Blanco Mera Granite properties.

Tensile strength, σ_t	6.1–9.7 MPa
Uniaxial compressive strength, σ_c	60.4–83.5
Young's modulus, E	30.64–33.0 GPa
Poisson's ratio, ν	0.16–0.20
Effective porosity, n_e	1.2–1.3 %
Mode I fracture toughness, K_{IC}	1.23 ± 0.03 MPa $m^{1/2}$

Tests were performed using cubic rock samples of 150mm-edge. Samples are prepared by drilling a vertical borehole up to the geometrical centre of the cube (~75 mm-length) starting from the centre of the top face using a 6-mm drill bit cooled with a water/cutting oil mixture (figure 1a). Then the borehole is cleaned, and the sample is oven-dried at 100ºC for 24 hours to remove the moisture content from the material. Then a 1/8" (~3.18 mm) stainless steel tube (aimed at conducting the hydrofracturing fluid during its injection) is introduced into the borehole up to a depth of ~50 mm (i.e., leaving a cavity of ~25 mm- length for fluid pressurization). The pipe is glued to the walls of the borehole using a two-component epoxy. Care was paid to ensure that the pipe remained vertically aligned and centred with respect to the borehole axis. The bottom part of the pipe is threaded. To prevent glue penetration into the pipe, a simple sealing system consisting of a coaxial flexible polymeric sleeve that is compressed between two nuts seals the contact with the rock (figure 1b). Finally, four 120-Ω strain gages are epoxy-glued onto the lateral surfaces of the samples in two orthogonal directions to measure strains during the tests (figure 1c). Magnets are also glued with cyanoacrylate to the surface of the specimen to attach the acoustic emission sensors. Prior to pressurizing the hydrofracturing fluid, the pipe is bent and filled with the fluid to remove any air gap existing inside.

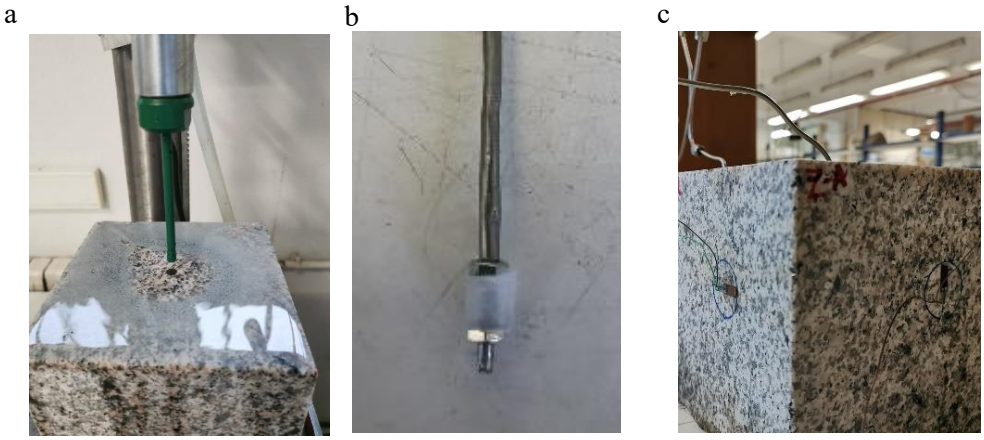

Figure 1. Sample preparation process: a) Borehole drilling; b) Detail of the edge of the pipe and sealing system; and c) Strain gages.

2.2. Experimental setup

Tests are executed in a high-strength, high-stiffness steel frame which allows to deliver independent lateral loads in two orthogonal horizontal directions (σ_H and σ_h). A hydraulic actuator associated with a

servo- hydraulic frame provides with the third, vertically-aligned loading axis (σ_V). Horizontal stresses are applied using two flat hydraulic cylinders (with a maximum nominal load of 150 t (~1471 kN)~) which are controlled by two dedicated syringe-type hydraulic pumps. The maximum capacity of the vertical hydraulic actuator is 1500 kN. Three linear variable differential transducers (LVDTs) attached to the loading plates using 3D printed special fixtures measure the bulk displacement operating over each axis of the specimen, while four strain gages measure the local strains directly over the surface of the sample. Although we measured continuously the displacements and strains in all the tests, their assessment is out of the scope of this work. The hydraulic fracturing fluid used is a mineral oil (HLP 32, ISO 6743/HM) that is delivered through the pipe using a high-pressure pump (Teledyne ISCO 100DX). The samples are placed in the centre of the frame and then laterally confined among four specially-designed Al plates and steel spacers. The loading plates have orifices to allow the insertion of up to nine AE sensors per plate and include a recess to avoid the compression of the glued strain gages. In addition, the back side of the plates have carved grooves to bypass the wires of the measuring devices (figures 2 and 3). Vertically, the sample is compressed between two steel plates having the one on the top a groove to conduct the pipe used for fluid injection. The edges of the six loading plates in contact with the sample are bevelled 5 mm to avoid interaction among adjacent faces. Therefore, the effective loading surface on a 150 mm-edge cube reduces to 140x140 mm^2, which corresponds to a maximum load capacity of the horizontal hydraulic cylinders on the samples of ~75 MPa, and ~76.5 MPa for the vertical hydraulic actuator. To decrease the rock-Al friction and reduce edge-effects, the plates were lubricated with a mixture of vaseline and stearic acid.

AE activity is recorded using a multichannel monitoring system (AMSY-6, Vallen Systeme GmbH, Germany) using four AE sensors (mod. VS700-D) on each plate perpendicular to σ_h. We use this 8-channel system to locate the AE events. The location of the sensors was chosen to improve fracture location during the tests (figure 4) [7-9]. A threshold of 30 dB was set for the tests without confinement. In the rest of the experiments that value was increased up to 55 dB to reduce noise coming from the testing system. Coupling between the AE sensors and the magnets was improved using a thin layer of silicone grease (OKS 1110). The AE signals were amplified using AEP5 preamplifiers set to a 34 dB-grain. We recorded AE time-based parameters (i.e., amplitude, counts, energy, etc.) with a sampling frequency rate of 10 MHz, and a band-pass digital filter configuration of 95–850 kHz.

Figure 2. The sample ready to be tested

2.3. Testing procedure

The testing procedure can be split into two consecutive stages: (1) the sample is triaxially loaded to the target stress conditions; and (2) the fluid is injected into the borehole to fracture the sample. Loading is performed stepwise. First, the load is increased simultaneously on the three axes until reaching the value of the minimum horizontal stress, σ_h (or the confining stress, $\sigma_{conf} = \sigma_h = \sigma_H = \sigma_V$, in hydrostatic tests). Then, keeping σ_h constant on one of the horizontal axes, the load is increased on the other two directions up to the value of the maximum horizontal stress, σ_H. Finally, maintaining the stress on the two horizontal axes constant, the load is increased on the third axis up to the value of the vertical stress, σ_V, reaching a normal stress regime condition ($\sigma_V \geq \sigma_H \geq \sigma_h$). The loading rate was adjusted so that the target stress was reached on 10 minutes on each step and, after that, the stress conditions were maintained

during 5 additional minutes to allow the mechanical stabilization of the system before proceeding to the next loading stage.
When the target stress conditions are reached on the three axes, the fluid injection stage starts. Injection is performed at a low-flow constant rate (0.025–0.10 mL/min) to avoid abrupt fracture propagation at breakdown pressure. After failure, fluid is re-injected into the sample to further propagate the fracture using the same or a larger flow rate than that leading to fracture onset (0.025–3.6 mL/min).

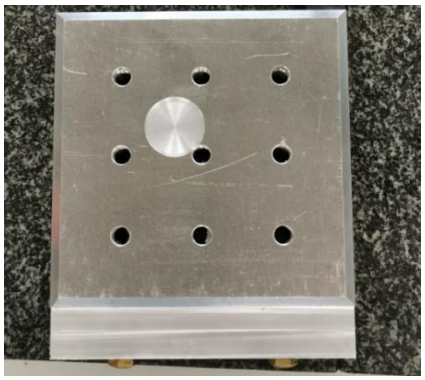

Figure 3. Detail of the inner surface of the Al plates, showing the 9-mm diameter perforations for the AE sensors and the 30-mm recess to protect strain gages.

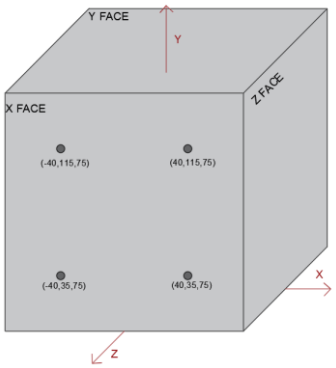

Figure 4. Location of the AE sensors. σ_V, σ_H and σ_h are applied on the Y, X and Z directions, respectively.

3. Results and discussion

In this study we report the results of 13 hydrofracturing tests: 2 hydrostatic tests without confining pressure, 5 hydrostatic tests with confining pressure (σ_{conf} = 10–35 MPa), and 6 normal stress regime ($\sigma_V > \sigma_H \geq \sigma_h$) tests. The associated stress conditions as well as values for the injection flow rates before failure (Q_{inj}) and breakdown pressures (P_{SB}) are compiled in table 2.

Table 2. Test conditions (σ_V = vertical stress applied on Y axis, σ_H = maximum horizontal stress applied on X axis, σ_h = minimum horizontal stress applied on Z axis, σ_{conf} = confining stress in hydrostatic tests, Q_{inj} = injection flow rate) and breakdown pressure (P_{SB}) values for the tests performed in this study.

	σ_V (MPa)	σ_H (MPa)	σ_h (MPa)	σ_{conf} (MPa)	Q_{inj} (mL/min)	P_{SB} (MPa)
T-11	-	-	-	0.10	0.050	16.17
1-S2	-	-	-	0.10	0.050	11.78
2-S2	-	-	-	10.00	0.025	18.11
T-4	-	-	-	15.00	0.050	26.76
3-S2	-	-	-	20.00	0.050	26.46
T-7	-	-	-	25.00	0.050	33.06
T-8	-	-	-	35.00	0.050	49.50
6-S2-1	12.50	10.00	5.00	-	0.050	19.32
6-S2-2	12.50	10.00	5.00	-	0.050	14.85
8-S2	22.50	10.00	9.00	-	0.050	15.15
T-9	25.00	10.00	10.00	-	0.050	12.58
7-S2	25.00	20.00	10.00	-	0.050	12.17
9-S2	45.00	20.00	18.00	-	0.100	33.39

3.1. Mechanical evolution

Figure 5 (top) shows the results of a hydrostatic test performed without confining pressure (i.e., σ_V = σ_H = σ_h = 0.1 MPa). First, oil was injected at a high flow rate of 1 mL/min until the pressure reached a value of ~2 MPa. Then, Q_{inj} was reduced to a lower rate of 0.05 mL/min to ensure a better control on

fracture propagation at failure. We observe that the injection pressure (P_{oil}) increases linearly up to ~95% P_{SB}, resulting in a short non-linear phase before the peak. After failure, the fracture produced in the material grows slowly, as suggested from the controlled decreased in pressure in the post-peak region. When the value of P_{oil} stabilizes (~1 MPa), fluid was injected again at a higher rate of 0.1 mL/min to further propagate the fracture. We observe that P_{oil} reaches a stable plateau at ~3 MPa, suggesting that this is the value of pressure that keeps the fracture barely open for the given flow condition [10]. The process is repeated at Q_{inj} =0.2 mL/min and, once more, P_{oil} stabilizes although at a higher pressure value (~5.5 MPa). Similarly, we plotted in figure 5 (bottom) the results of a non-hydrostatic test under normal stress regime. In this case, we observe the stepwise loading increase (t < 0 min) with the corresponding stabilization stages. After 45 minutes (t = 0 min), fluid injection started at a rate of 0.10 mL/min. Like in the previous case, P_{oil} increased almost linearly up to P_{SB} and, following failure, fracture propagation is controlled. Although it was expected that P_{oil} stabilized at a pressure close to σ_h [11], we observe that the value reached is lower (~15 MPa). After a period in which injection was stopped, fluid was reinjected at the same flow rate. The difference between the values of peak pressure from the two injection stages would reflect the tensile strength of the material [12]. From our results we derive a value of σ_t ~ 11.6 MPa for the Blanco Mera granite, which is slightly larger than that reported in table 1 for indirect (Brazilian) tensile tests.

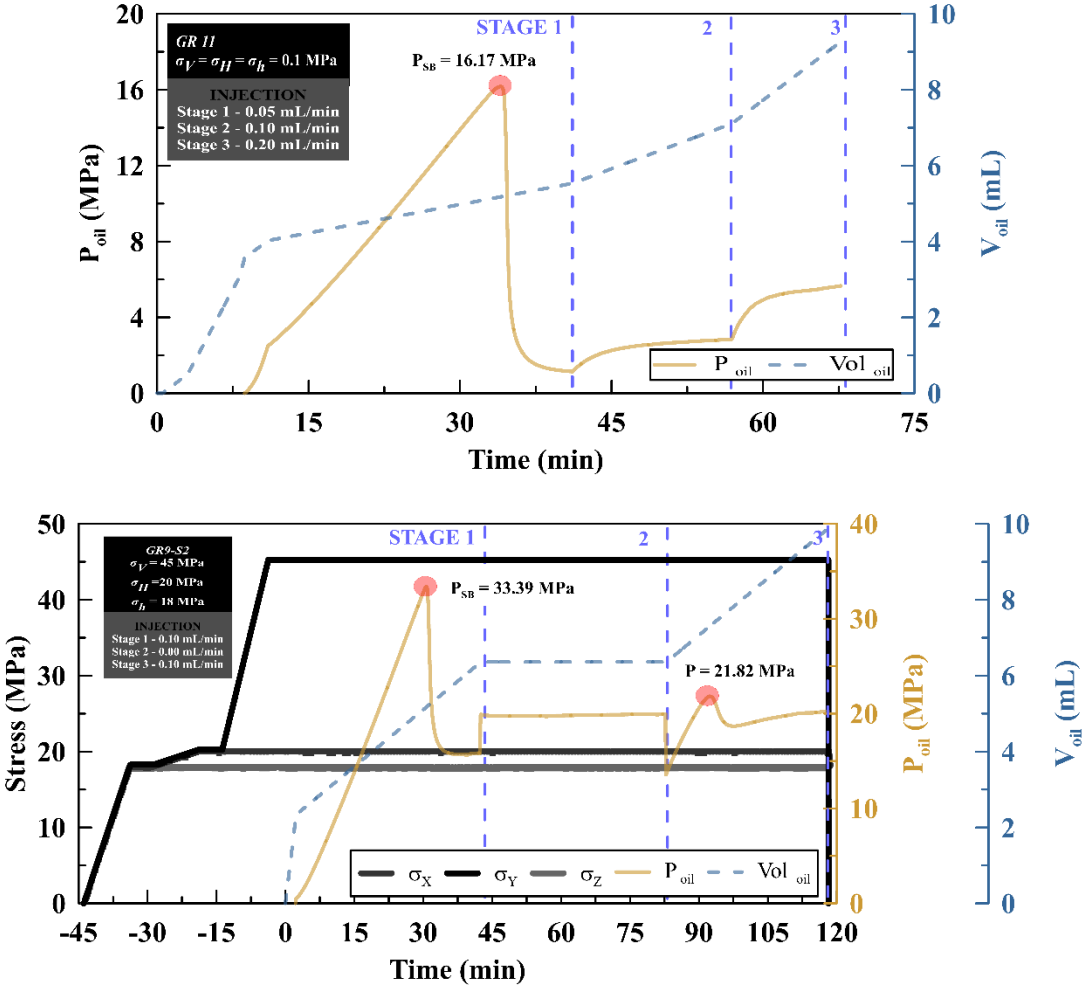

Figure 5. Evolution of injection pressure (P_{oil}) and volume (V_{oil}) in selected unconfined hydrostatic (T-11; top) and normal stress regime (9-S2; bottom) tests. For the latter, the stress evolution in the three axes (σ_V, σ_H and σ_h) is also displayed. Dashed lines separate injection stages (1, 2 and 3). The horizontal axis is set so that t = 0 is the time at which fluid injection starts.

3.2. Breakdown pressure assessment

The time evolution of the injection pressure (P_{oil}) during five selected hydrofracturing tests performed in this study is displayed in figure 6. We observe a dependence of the slope of the curves on the flow rate, with higher rates resulting in steeper curves. However, it seems that the stress state at which the sample is subjected has no influence on the rate of pressure increase, as suggested by the parallelism of the curves obtained for equal Q_{inj}.

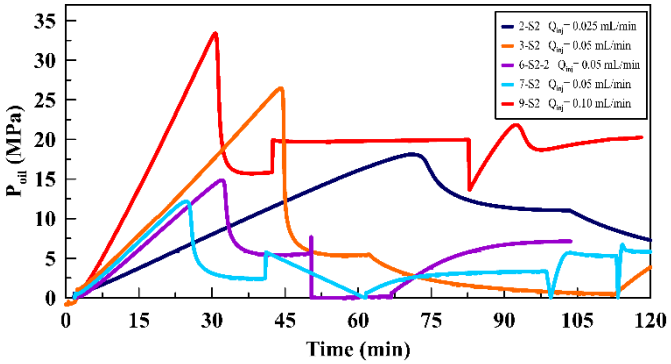

Figure 6. Time evolution of the injection pressure (P_{oil}) during five selected tests. The corresponding injection flow rates before failure (Q_{inj}) are given in the legend.

For hydrostatic open-hole experiments performed with four different rock types, Stöeckhert [13] reported a nearly one-to-one relationship between breakdown pressure and confining pressure, such that:

$$P_{SB} \approx \sigma_{conf} + P_{SB}^{0}$$

where P^{0}_{SB} corresponds to the intercept of the linear fitting with the pressure axis. Following this approach, in figure 8 (left) we plot the values of P_{SB} resulting from the hydrostatic (unconfined and confined) tests as a function of the applied stress (σ_{conf}). The obtained slope from the linear fitting (0.94) is in good agreement with the results reported in [14]. However, it must be noted that the pressurization volume in open-hole experiments (which corresponds to a section along the whole specimen length) differs from that of the hydrofrac tests reported in this work (~25 mm- length for a 150-mm edge cubic sample). The value of $P_{SB,0}$ (i.e., the breakdown pressure at no confining pressure) might be related with the tensile strength (σ_t) of the material. However, Stöeckhert [13] has observed slightly larger values of $P_{SB,0}$ compared with the magnitudes of σ_t determined in Brazilian tests. This is also observed for the samples of Blanco Mera granite tested in this study ($P_{SB,0}$ = 11.8 MPa). It is interesting to observe that the values of tensile strength derived in this work from two different approaches (that from the linear fitting in hydrostatic tests, $P_{SB,0}$, and that from the peak pressure difference during fluid injection) are in good agreement.

In the non-hydrostatic tests, hydraulic fractures are generally created perpendicular to the least principal stress, as show in figure 7. Thus, we may expect to find a relation between the breakdown pressure (that produces rock sample fracturing) and the minimum applied stress, which corresponds to σ_h in our experiments. To check this conjecture, in figure 8 we represent the values of P_{SB} recorded in normal stress regime tests as a function of σ_h. Our results would suggest that breakdown pressure tends to increase with increasing stress, although both parameters show no clear correlation (R^2 = 0.50).

3.3. Acoustic emission activity

Results of cumulative acoustic emission energy (E_{AE}) and amplitude are plotted as a function of time in figure 9 for a hydrostatic test with no confining pressure. The injection pressure curve is also displayed in the same figure as reference. In the pre-peak region, very low AE activity was recorded. However, at breakdown pressure we observe a large number of high energy and amplitude events, what would suggest the onset of fracturing [14]. As the pressure decreases in the post-peak, the amplitude of the

events progressively decreases. Molenda et al [15] related this behaviour to fracture closure. With the AE data recorded, we also computed the hypocentre location of the AE events using Vallen software considering a constant velocity field (v ~ 2500 m/s) in the material. To try to illustrate the crack growing process, in figure 9 we have represented those events with an amplitude greater than 45 dB in two different time windows after P_{SB}. Our results show that, right after P_{SB}, the events mainly locate in the region next to the borehole, and that they extend upwards, as previously reported in [16].

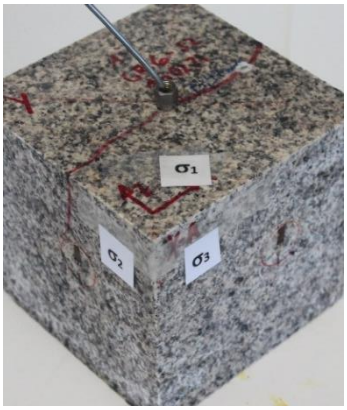

Figure 7. Hydraulic fracture in Test 6-S2-1. The fracture is perpendicular to σ_h (σ_3 in the picture).

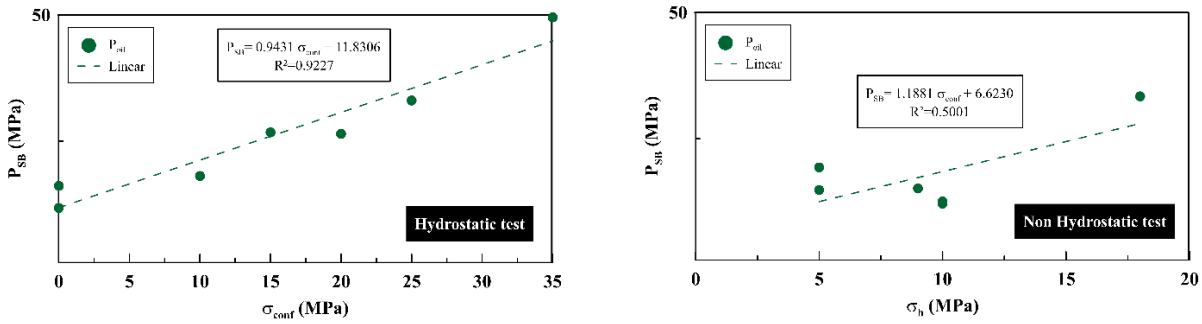

Figure 8. Breakdown pressure (P_{SB}) as a function of confining stress (σ_{conf}) in hydrostacic tests (left); and breakdown pressure (P_{SB}) as a function of minimum horizontal stress (σ_h) in non-hydrostatic tests (right).

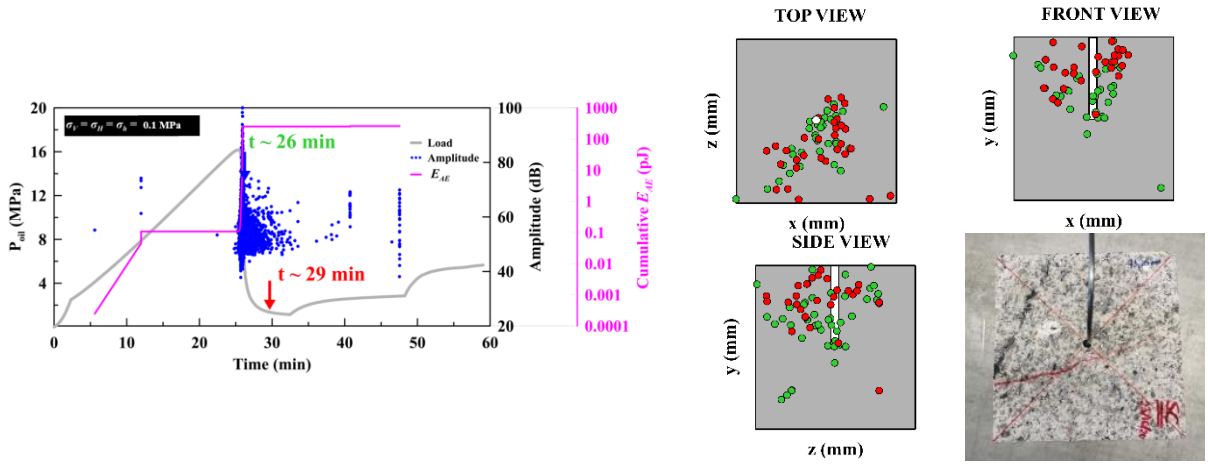

Figure 9. AE results for sample T-11. On the left: Injection pressure (P_{oil}), amplitude and cumulative AE energy vs time. On the right: Location of the AE events (3 views, green and red dots represent t~26 min and t~29 min) and a top view of the actual fractured sample.

4. Conclusions

We report the results of 13 hydraulic fracturing test performed under true triaxial conditions using cubic samples of Blanco Mera granite. Tests were carried out in a high-strength, high-stiffness steel frame, associated with a servo-hydraulic frame. Our results suggest a nearly one relationship between breakdown pressure and confining stress in hydrostatic experiments. In addition, the value of tensile strength derived from the linear fitting of the hydrostatic tests ($P_{SB,0}$ = 11.8 MPa), although slightly lower than that reported previously for Brazilian tests, is in good agreement with that computed from the peak pressure analysis during injection(σ_t ~ 11.6 MPa). According to the location of the AE events, the hydraulic fracture propagates from the bottom of the borehole upwards. Although we relate this behaviour to the presence of a region of weakness surrounding the well, further work would be needed to assess the influence of the relative orientation of the perforation and the principal stresses.

Acknowledgements

This work was funded by Repsol S.A. and the MINECO/AEI/FEDER, UE project BIA2017- 87066-R. The authors would like to thank Dr. Leandro Alejano-Monge for his advice.

References

[1] Boudet H, Bugden D, Zanocco C and Maibach E 2016 *Environ. Politics* **25** 593-612
[2] Clark, J B 1949 *J. Pet. Technol.* **1** 1-8
[3] Muñoz-Ibáñez A, Delgado-Martín J, Juncosa-Rivera R., Romera-Rodríguez L, Alejano-Monge L, Canal-Vila J, González-Molano N, Alvarellos-Iglesias J, López-Puiggene Eand Lakshmikantha M R 2019 *Proc. Int. Cong. on Rock Mechanics and Rock Engineering (Foz do Iguassu)* (Leiden: The Netherlands/CRC Press)pp 1195-1202.
[4] Muñoz-Ibáñez A, Delgado-Martín J and Juncosa-Rivera R 2021 *Int. J. Rock Mech. Min. Sci.* **143C** 104785
[5] Arzúa J 2015 *Dilation in granite during servo-controlled triaxial strength tests* (University of Vigo, Spain)
[6] Muñoz-Ibáñez A, Delgado-Martín J, Costas M, Rabuñal-Dopico J, Alvarellos-Iglesias J and Canal-Vila Jacobo 2020 Pure Mode I Fracture Toughness Determination in Rocks Using a Pseudo-Compact Tension (pCT) Test Approach *Rock Mech. Rock Eng.* **53** 3267-85
[7] Johnson E and Cleary M P 1991 *Proc. of the SPE Low Permeability Reservoirs Symposium* pp 413–28
[8] Perkins T W and Kern L R 1961 *Pet. Tech.* **13** 937–49
[9] Warpinski N R, Clark J A, Schmidt R A and Huddle C W 1982 *SPE J.* **22** 333–40
[10] Springer J E, Qingshan Z, Haimson B C, Zobac M D, Lee M Y and Fangquan L 1987 In-situ stress project, technical report number 9: Interpretation of hydraulic fracturing data from Yongping, Western Yunnan, China. *Department of the Interior, U.S. Geological Survey*
[11] Haimson B C and Cornet F H 2003 *Int. J. Rock Mech. Min. Sci. Geomech. Abstr* **40** 1011-20
[12] Goodman R 1989 *Introduction to rock mechanics* (Canada) p 120
[13] Stöckhert F 2015 Fracture Mechanics applied to Hydraulic Fracturing in Laboratory Experiments *RuhrUniversitat Bochum*
[14] Moradian Z, Einstein H, Ballivy G 2016 *Rock Mech Rock Eng* **49** 785-800
[15] Molenda M, Stöckhert F., Brenne S and Alber M 2015 *31st Conference of the European Working Group on Acoustic Emission* (Dresden: Germany)
[16] Zhuang L, Jung S G, Diaz M, Kim K Y, Hofmann H, Min K B, Zang A, Stephansson O, Zimmermann G and Yoon J S 2020 *Rock Mech Rock Eng* **53** 4329-44